Chemical Engineering Science 320 (2026) 122402

Contents lists available at ScienceDirect

Chemical Engineering Science

journal homepage: www.elsevier.com/locate/ces

Hard and thermally stable NiW-graphite balls composite coatings via anode consumed co-electro-deposition

Zhifei Yu [a], Xingwen Zhang [a], Zhan Liu [a], Shaojia Shi [a], Qingzhong Mao [a,b], Yonghao Zhao [a,b,*], Zesheng You [c,*]

[a] Nano and Heterogeneous Materials Center, School of Materials Science and Engineering, Nanjing University of Science and Technology, Nanjing 210094, China
[b] School of Materials Science and Engineering, Hohai University, Changzhou 213200, China
[c] Herbert Gleiter Institute of Nanoscience, School of Materials Science and Engineering, Nanjing University of Science and Technology, Nanjing 210094, China

ARTICLE INFO

Keywords:
NiW electrodeposition
Graphite anode
Anode consumed co-electro-deposition
Composite coatings
Hardness and thermal stability

ABSTRACT

Surface treatments, for instance the electrodeposition, have the capability to shield the internal substrate from extreme environments. Recently, the integration of composite fillers into electroplating coatings has emerged as a crucial strategy for enhancing mechanical properties. However, it inevitably involves adding particles while overlooked contribution of anode. Here, firstly, we electroplated NiW coatings on 30CrNi2MoV steel, obtained coatings with different tungsten (W) contents from 6.4 wt% to 45.1 wt% by changing the current density from 0.10 A·cm^{-2} to 0.35 A·cm^{-2} and medium temperature from 60 °C to 90 °C, accordingly the hardness was from 540HV to 795HV. Secondly, prepared NiW-graphite balls (GBs) composite coatings by one-step graphite anode consumption co-electro-deposition (ACCED) technology appending the varieties amount GBs into NiW alloy via adjusting temperature and current density. The hardness and thermal stability of the composite coating obtained by this process can reach 853HV, and the highest hardening rate can reach 20.29% at a GBs proportion of 3.93%. Simultaneously, the surface hardness of NiW-GBs composite coatings by ACCED remains elevated even following prolonged high-temperature annealing. Finally, the contributions of W atom solid solution hardening and GBs doping strengthening in NiW electrodeposited composite coatings were analyzed and quantified. GBs tend to be released from anode and co-deposit under conditions of high current density and temperature. This work introduces a single-step anode consumption co-deposition technique that directly combines NiW with GBs to create a coating possessing high hardness and thermal stability, providing valuable insights for related fields.

1. Introduction

Surface electroplating technology involves depositing a high-performance coating onto the surface of a substrate to address the challenges posed by harsh service environments and performance application requirements. In industries such as automotive, aerospace, nuclear energy, and electronics, materials are subjected to severe mechanical and environmental pressures. Therefore, mechanical properties such as strength and thermal stability are important concerns of structural materials. Surface treatments, particularly metal coatings, have been widely applied to meet these requirements (Figuet et al., 2022; Dash and Panda, 2024). Because it is difficult to obtain materials that can perfectly balance performance in applications, surface treatment and composite methods are commonly led to pursue overall properties. However, traditional composite methods are inevitably restricted to the addition of particles to the electrodeposition solution system, making it challenging to implement other modifications. Additionally, during the electrodeposition process, the anode is typically viewed as a standard connecting component, and its consumption and contributions are rarely under consideration. In the realm of artillery tubes, the thermal-pressure coupling effect is pivotal in inducing cracking or delamination failures within surface electrodeposited coating technology. Consequently, the ultra-high requirements for strength and thermal stability of surface coating materials emerge as the most critical performance indicators (Geng et al., 2023; Liao et al., 2014). Moreover, the process requirements for large-caliber gun barrels (tens of meters) make tons of electroplating solution high consumption a critical factor in controlling costs. Consequently, the introduction of a substantial quantity of

* Corresponding authors at: Nano and Heterogeneous Materials Center, School of Materials Science and Engineering, Nanjing University of Science and Technology, Nanjing 210094, China (Qingzhong Mao).
E-mail addresses: yhzhao@njust.edu.cn (Y. Zhao), zsyou@njust.edu.cn (Z. You).

https://doi.org/10.1016/j.ces.2025.122402
Received 15 June 2025; Received in revised form 26 July 2025; Accepted 10 August 2025
Available online 11 August 2025

composite particles becomes impractical, and the essential consumption of the anode warrants attention. In electrodeposition process, the anodic oxidation or consumption changes solution status under different electrical regime, especially in high current density or voltage (Sieber et al., 2016). The indispensable anode can be utilized as the key component to provide composite particles into electrodeposition solution for enhancement. Additionally, as a substrate, the surface chrome electroplating of the inner lining on gun barrels has become the most prevalent treatment method due to its high hardness and wear resistance, nevertheless, the toxicity and environmental hazards associated with Cr^{6+}, in addition to the inevitable microcracks in chromium coating that accelerate failure, necessitate the exploration of alternative materials exhibiting superior performance (Pierre et al., 2008; Saravanan and Mohan, 2009).

Nanocrystalline-nickel (Nc-Ni) electrodeposition processes are well-established for scientific and engineering applications. However, the application of Nc-Ni is limited due to its low starting temperature of grain growth, which can be as low as 250 °C (Klement et al., 2009). On this basis, the application of Nc-Ni electrodeposition prosses is certainly limited due to the insufficient grain boundary stability and time-dependent plastic deformation. Nevertheless, the addition of refractory metals (such as W, Mo or Ta) to form alloys can suppress grain boundary diffusion, furthermore achieve significant enhancement of grain structure and mechanical properties (Hasegawa et al., 2017). In this regard, the electrodeposition of Nickel-Tungsten (NiW) alloy has attracted considerable interest due to its unique characteristics that the combination of thermal stability and superior mechanical performance (Detor and Schuh, 2007; Schuh et al., 2003). Nowadays, NiW alloys prepared by electrodeposition technology have been researched for period time. Due to its exceptionally high hardness, NiW alloy is considered as a new alternative to conventional chromium plating technology. Furthermore, its superior thermal stability renders it particularly well-suited for use as lining materials in artillery. Therefore, recent research has also focused on optimizing the process of NiW alloy coatings to improve their mechanical properties especially about matching of strength and thermal stability aiming to achieve higher operating conditions.

Composition and modification are known as effective method to achieve better performance and optimize application effectiveness. Co-electrodeposition process, whereby ceramic or organic particles are simultaneously deposited with metal ions on a substrate, has been a subject of interest in the surface coating community, as the obtained composites often show enhanced hardness and structure stability (Low et al., 2006). Among them, the co-electrodeposited NiW composite coatings have been demonstrated to possess superior mechanical, wear-resistant, and corrosion-resistant properties. Currently, substantial efforts have been made to prepare NiW composite coatings using traditional co-deposition processes. Cheng et al. appended PDA-functionalized h-BN nanosheets into NiW coatings which improved hardness, wear resistance and corrosion resistance properties (Cheng et al., 2024). Liu et al. produced NiW/SiO_2 nano composite coating by electrodeposition which obtained hard surface (up to 643.23 HV) and reduced corrosion rate to 9.7 μA/cm^2 (Xijing and Yong, 2023). Wang et al. concluded that the hardness of NiW alloy and NiW/diamond composite coating increases obviously when heated at 500 °C and 600 °C due to the crystallization of Ni and precipitation of Ni_4W phase. For the Ni–W/diamond composite coating with diamond content of 21 ± 1 vol% hardness can reach to 1205 HV after annealing at 600 °C (Wang et al., 2014). Liao et al. composited NiW coatings and micro and nano SiC respectively. The introduction of micro-SiC particles have ability to improve the wear resistance of NiW coating and reduce the oxidative wear and peeling (Liao et al., 2022). Lanzutti et al. produced Ni matrix micro- and nano SiC composite coatings by pulse current electrodeposition and explored the wear behavior. It demonstrated that micro composite coatings exhibited a harder surface compared to nano composition when subjected to low-frequency pulse electrodeposition at frequencies of 0.01, 0.1 and 1 Hz. Consequently, the wear resistance of the coatings was also enhanced (Lanzutti et al., 2019). Numerous research has consistently proved that variations in particle composition scale leads to differences in performance improvements (Lanzutti et al., 2019; Lekka et al., 2012). In this case, select the appropriate compound for composite reinforcement is of critical significance. Moreover, simplifying the synthesis process and managing industrial costs hold significant research implications.

Despite the excellent properties of carbon materials, such as diamond, graphene, carbon nanotubes, and carbon fibers, as reinforcements for composites, the high level of incorporation, agglomeration, and poor dispersion within the matrix can unfortunately degrade the mechanical properties of the materials (Uysal et al., 2021). Therefore, screening the type, dosage, and particle size of fillers is critical factor to obtaining composite coatings with excellent compatibility. Graphite commonly used as anodes in electrodeposition technology, are readily accessible as well as cost-effective and find applications in the composites field in order to refine grain size and enhance mechanical properties such as strength, wear resistance or thermal stability (Chen et al., 2025; Ren et al., 2025). Its particle size can be controlled within the optimal range from a few micrometers to nanometers, ensuring the best reinforcement. Consequently, the design of an electrodeposition process utilizing graphite as the anode involves the continuous release of graphite particles into the electrodeposited system through temperature or current density adjustments. These particles are subsequently co-deposited at the cathode to create composite alloy coatings, thereby facilitating the efficient and cost-effective preparation of graphite particle-reinforced alloy coatings.

In this work, we first proposed the graphite anode consumed co-electro-deposition (ACCED) technology i.e., designed and utilized to one-step synthesis NiW-graphite balls (GBs) composite coatings under adjusting process parameter to control the added amount. The hardness and thermal stability of composite coatings were tested and studied and comparing to the pure NiW alloys. Moreover, employing interpolation, extrapolation, and computational verification methods, the ACCED mechanism of graphite anodes was validated. The specific mechanisms that enhance the mechanical properties of solid solutions and composite reinforcements are analyzed separately.

2. 2.Experimental

2.1. Chemical and materials

Sodium hydroxide (NaOH), Sodium carbonate (Na_2CO_3), Sodium phosphate (Na_3PO_4) and lauryl sodium sulfate (SDS) for substrate pre-degreased, hydrochloric acid (HCl) for activation and nickel sulfate hexahydrate ($NiSO_4{\cdot}6H_2O$), sodium tungstate dihydrate ($Na_2WO_4{\cdot}2H_2O$), sodium citrate dihydrate ($Na_3C_6H_5O_7{\cdot}2H_2O$), ammonium chloride ($NH_4Cl$), sodium bromide (NaBr) as electrodeposition medium were purchased from Sinopharm Chemical Reagent Co., Ltd. All reagents were used without further purification. 30CrNi2MoV steel commonly used as the basement of gun barrels served as the substrate material for the electrodeposition. The dimensions of the substrate designated for plating are 30 × 10 × 1 mm and its chemical composition analysis result is shown in Table S1. The anode was selected as either pure nickel or graphite plate with a purity of 99.9 %. Both dimensions measure 60 × 70 × 3 mm.

2.2. Pre-treatment of substrates

To achieve a flat and smooth surface, the surface of the 30CrNi2MoV steel to be plated underwent a sequential polishing process using 80#, 600#, 1500#, and 2000# sandpaper. Following this, a diamond abrasive pastes with a grain size of 1.0 μm was applied and polished until a mirror-like finish was obtained. Finally, the surface was thoroughly ultrasonic rinsed with deionized water and ethyl alcohol for 10 min respectively. Pre-treatment process as an electrodeposition substrate

was as following: the steel coupon was immersed in degreased fluid at 50 °C for 10 min. After rinsing with deionized water, immerse the coupon in a 2 wt% HCl for 3 min for activation. Finally, thoroughly rinsed and dried the coupon.

2.3. Preparation of NiW and composite coatings

The electrodeposition was carried out in a plating bath utilizing specific aqueous bath chemistry. The composition of the deposition medium, including the ingredients and their respective concentrations, is presented in Table 1 below. The direct current electrodeposition device diagram and concept of ACCED technology can be seen in Fig. 1, illustrating the fabrication process of NiW alloy optimize to NiW-GBs composition coating through a one-step ACCED method. In this process, the 30CrNi2MoV cathode was submerged in the electroplating solution, while the anode was positioned opposite to the surface of the cathode, with a spacing of 4 cm. The current for electrodeposition process was regulated by power supply (SOYI-3010DM) purchased from Shanghai Soyi Electronic Technology Co., LTD. During the initial stage of the electrodeposition process, the direct current ramped up to the set value at a rate of 10^{-3} A·s^{-1}. It is noteworthy that for each preparation of coating, a fresh electroplating medium was utilized. Hence, the failure caused by the consumption of solution can be eliminated and demonstrated that GBs released from graphite anode is continuously effective.

2.4. Microstructural characterizations

Surface morphology of coatings was observed by optical microscope (OM, BX41M-LED) and scanning electron microscope (SEM, Quanta 250F). Elemental compositions specifically W content was appraised on a field emission SEM equipped with Oxford energy dispersive X-ray spectrometer (EDS). Three random regions were characterized for determining error bars. X-ray diffractometer (XRD) by a Bruker D8 was carried out with Cu–Kα radiation between 20° and 100° to analyze the phase structures of coatings. Crystallite size was calculated from Ni (111) peak at around $2\theta = 44.1°$ of NiW alloys, after correcting for instrumental broadening under support of Scherrer formula. The microstructures were characterized on Aberration correction transmission electron microscopy at sub-Angstrom resolution (Titan G2 60–300) and samples for high resolution transmission electron microscopy (HR-TEM) observation were prepared by focused ion beam (FIB) system in order to statistical grain size. The microstructure of samples was investigated qualitatively by ex-situ cross-sectional FIB observation.

2.5. Hardness and strength measurements

The Vickers hardness of the coating surface was evaluated using an HMV-G 21DT digital tester. The measurements follow the standard test method for micro indentation hardness of materials (ASTM E384-22). A load of 980.7 mN (HV 0.1KgF) was applied for a duration of 15 s during the indentation tests. Subsequently, HV is unified as the hardness unit. Randomly selected sites on each sample were tested, with a minimum of 8 tests conducted on each specimen to ensure repeatability. The average value and error bars were determined from these multiple tests. The hardness and elastic modulus of the samples were calculated using the Oliver–Pharr method (Su et al., 2018). The wear tests at room temperature and relative humidity maintained at 35 ± 5 % were carried on a tribometer (UMT-II, Germany). The sliding stroke and speed was set at 1 mm and 8 mm/s, respectively. Normal loads of 10 N were applied in the wear tests and sustained for 1 h. The Φ6 mm Al_2O_3 ball with a hardness of 1650 HV is selected as counter-body. The morphology of the wear scars was characterized by Confocal laser scanning microscope (CLSM, OLS4100).

Table 1
Composition of medium and deposition parameters.

$NiSO_4{\cdot}6H_2O$	15.78 g·L^{-1}	pH	8.5
$Na_2WO_4{\cdot}2H_2O$	25.41 g·L^{-1}	Temperature (°C)	60–90
$Na_3C_6H_5O_7{\cdot}2H_2O$	117.6 g·L^{-1}	Time (min)	60
NH_4CL	26.75 g·L^{-1}	Current density (A·cm^{-2})	0.05–0.35
NaBr	15.45 g·L^{-1}	Current ramp-up (A·s^{-1})	10^{-3}
Anode	Nickel/Graphite	Rotation rate (rpm)	1500

2.6. Thermal stability testing

In order to study the thermal stability of NiW coatings and application in extreme environments, the specimens were annealed at 400, 600, 800 °C in a tube furnace under a protective atmosphere of Ar atmosphere and duration for durations of 0.5, 1 and 2 h, respectively. To ensure that the changes in microstructure were exclusively attributed to the heat treatment rather than subtle microstructural differences among samples, one specimen from each condition was cut into blocks using an electrical discharge wire cutting machine with each block subsequently annealed at varying temperatures or aging times. Thermal stability is assessed by examining changes in hardness and comparing them to the initial value as deposited.

3. 3.Results

3.1. Electrodeposition of NiW coatings

3.1.1. Composition of NiW electrodeposited coatings

The composition of NiW coating is the primary factor that significantly influences its structural properties. Research has demonstrated that increasing the W content and solid solution decreases the grain size of nickel. Once the composition reaches 40 wt%, the nanocrystals undergo a transformation into amorphous (Yamasaki, 2001). Currently, the research efforts were concentrated on W-rich NiW alloys, and there is a scarcity of studies on NiW with low W content. Consequently, it is of utmost importance to conduct a comprehensive investigation into a broad range of W content. By frequently adjusting the manufacturing parameters of NiW thin film including temperature and current density, it becomes possible to directly achieve coatings with varying W contents. Here, NiW_x is served to describe the electrodeposition NiW alloy samples, where x indicates the percentage of W mass fraction. EDS analysis was charactered to determine W content. The NiW coating prepared at an exceptionally high current density (0.35 A·cm^{-2}) at 75 °C is likely to contain extremely high W content. Its SEM and EDS analysis images are shown in Fig. 2(a) and (b) respectively. Despite the high level of W content (45.1 wt%) the distribution of Ni and W elements on the surface is uniform and aggregation rarely. The composition of all other NiW coatings was determined through EDS analysis. NiW alloy coatings obtained with a pure nickel anode and there is no introduction of impurities element in the electrodeposition medium.

The tungsten content and microstructure are critical factors influencing performance, with process parameters known to impact the properties of electrodeposition. After determining the composition of the plating solution, temperature and current density emerge as the most crucial process parameters. Typically, high current density can result in enhanced W content and hardness in the plated layer (Eliaz et al., 2005). However, concerning temperature, there have been varied and, in some cases, conflicting reports on the effects of temperature on NiW coatings properties (Mizushima et al., 2005). While most studies indicate that increasing temperature led to a corresponding rise in W content, finer grains, more random orientation in NiW coatings, and improved faradaic cathodic current efficiency (Schuh et al., 2002; Sriraman et al., 2006; Sassi et al., 2012), some suggest that temperature had no significant impact on W content (Giga et al., 2006; Huang et al., 2021; Munagala et al., 2023). However, in this study, the intricate relationship among W content, temperature, and current density was unveiled through a comprehensive analysis of controlled electroplating parameters. Fig. 2(c) illustrated the W content of NiW coatings prepared under a

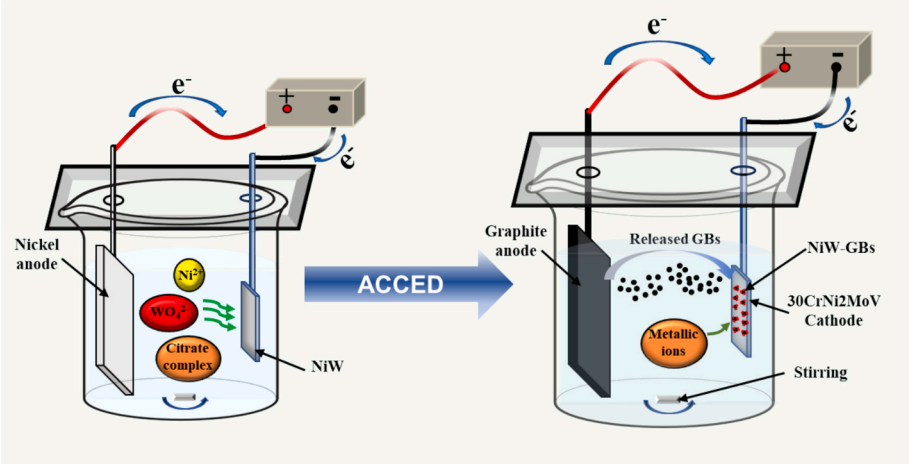

Fig. 1. Concept and device diagram of NiW-GBs composite coatings via ACCED.

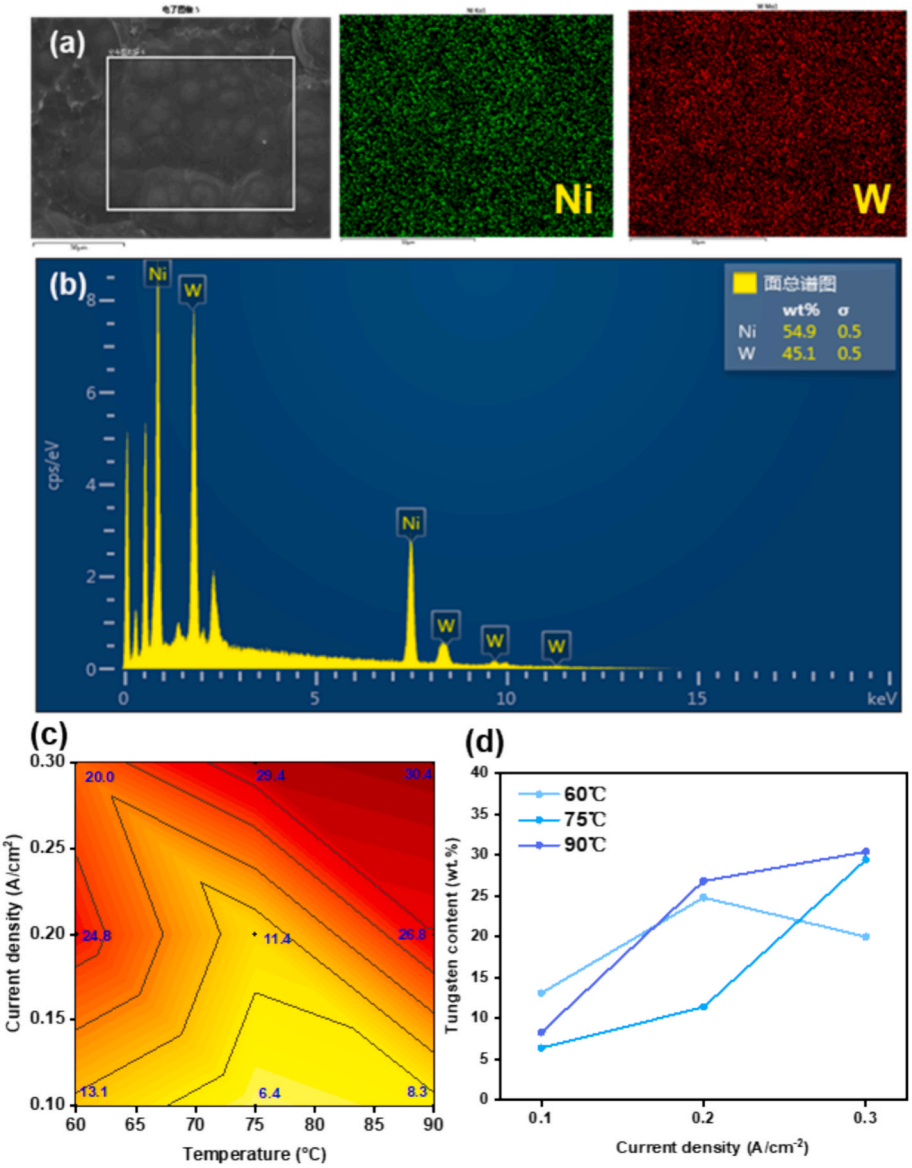

Fig. 2. Images of EDS mapping (a) and element content (b) of $NiW_{45.1}$. Distribution mapping and relationship of W content with temperature and current density (c) and (d).

wide range of temperature (60 °C–90 °C) and current density (0.1 A·cm^{-2}–0.3 A·cm^{-2}) conditions. As the temperature and current density increase, the color in the image intensifies, indicating a corresponding increase in tungsten content. For Fig. 2(d), at an electrodeposition medium temperature of 60 °C, there is no linear correlation between W content and current density. Within the temperature at 75 and 90 °C, an increase in current density led to higher W content. The Lowest W content of 6.4 wt% is observed at 0.1 A·cm^{-2} under 75 °C, which added significantly with the increase of current density and the most W content reaching 30.4 wt% at 90 °C and 0.3 A·cm^{-2}. The W content of NiW coatings prepared at 60 °C is generally maintained at a high level (10-30 wt%) and does not exhibit a direct correlation with current density. The reason is that in ammonia-containing electrodeposition systems, an increase in temperature (above 60 °C) may lead to decomposition and a reduction in pH. At this juncture, current density becomes the primary factor influencing deposition, and tungsten content exhibits a linear relationship with current density while higher W content obtained at 60 °C. Hence, the traditional cognition that single-factor changes can alter the properties of NiW coating is reasonable but only effective within a higher temperature range (75–90°C) (Somekawa et al., 2004; Allahyarzadeh et al., 2016). The W content in NiW coatings is jointly regulated by high temperature and current density factors, exhibiting control effectiveness within a limited range.

3.1.2. Surface morphology of NiW electrodeposited coatings

The surface morphology, structure, and flatness of electroplated coatings to some extent affect their application performance. The crystalline properties and grain sizes are changed by the influence of W content, and further, the surface morphology also exhibits differences. SEM top-view images of NiW electrodeposited coatings which W content progressively increases, with the corresponding figures labeled (a1) through (a9) arranged in sequence in Fig. 3. As shown in Fig. 3(a2)–(a4), when the mass fraction of W reaches 8.3 wt%, the surface morphology of Ni-rich NiW coating is composed of many spherical particles with the dimension around 300 nm, which formed by the aggregation of hundreds of nanocrystals arranging according to the law of bar shape in 2D scale. This is related to the polishing line of the electroplating substrate. With the increase of W content to 13.1 wt%, the particle size of the spherical particles increases somewhat consist with experimental result (Munagala et al., 2023). When the W content exceeds 20.0 wt%, the shape becomes dense islands, and then the surface structure of the W-rich NiW coating became myrmekitic texture which size has increased to several tens of micrometers. Furthermore, in traditional cognition, during the electrodeposition of NiW, the adsorption and inclusion of hydrogen in the deposits led to elevated internal stress, ultimately causing the formation of cracks (Alimadadi et al., 2009; Eliaz et al., 2005). While no cracks were detected on the surface of NiW coatings produced during the manufacturing process of this study so that address the limitation of application (Mizushima et al., 2005).

3.1.3. Microstructure of NiW electrodeposited coatings

TEM was employed to characterize the microstructure of NiW alloy electrodeposited coatings, specifically for the $NiW_{8.3}$, $NiW_{24.8}$, and W-rich $NiW_{35.5}$ in an amorphous state. The grain size of the nanocrystalline NiW was then calculated. The results are shown in Fig. 4. For the $NiW_{8.3}$ with lower W content, the grain size of face-centered cubic (FCC) Ni(W) is 9.2 ± 1.9 nm, while when for $NiW_{24.8}$ the amount of W in solid solution increases, the grains are refined to 8.2 ± 2.1 nm. The grain size of the nanocrystalline NiW alloy coatings remains within the parameters of Hall-Petch refined grain strengthening relationship, and has not exceeded the critical value of the anomalous relationship (Schuh et al., 2002; Sriraman et al., 2006). The secondary image illustrates electron diffraction spot images, where the electron diffraction spots of nanocrystalline NiW alloys are observed to form continuous rings. These rings are indicative of the diffraction results produced by numerous fine grains. However, for the NiW alloy produced in this study, as the W content increased to 36 wt%, the nanocrystals transformed into a disordered amorphous state. The electron diffraction pattern appears as an amorphous diffraction spot.

3.2. NiW-GBs composite coatings by ACCED

3.2.1. Morphology and composition of NiW-GBs

Graphite electrodes are composed of graphite particles, which have

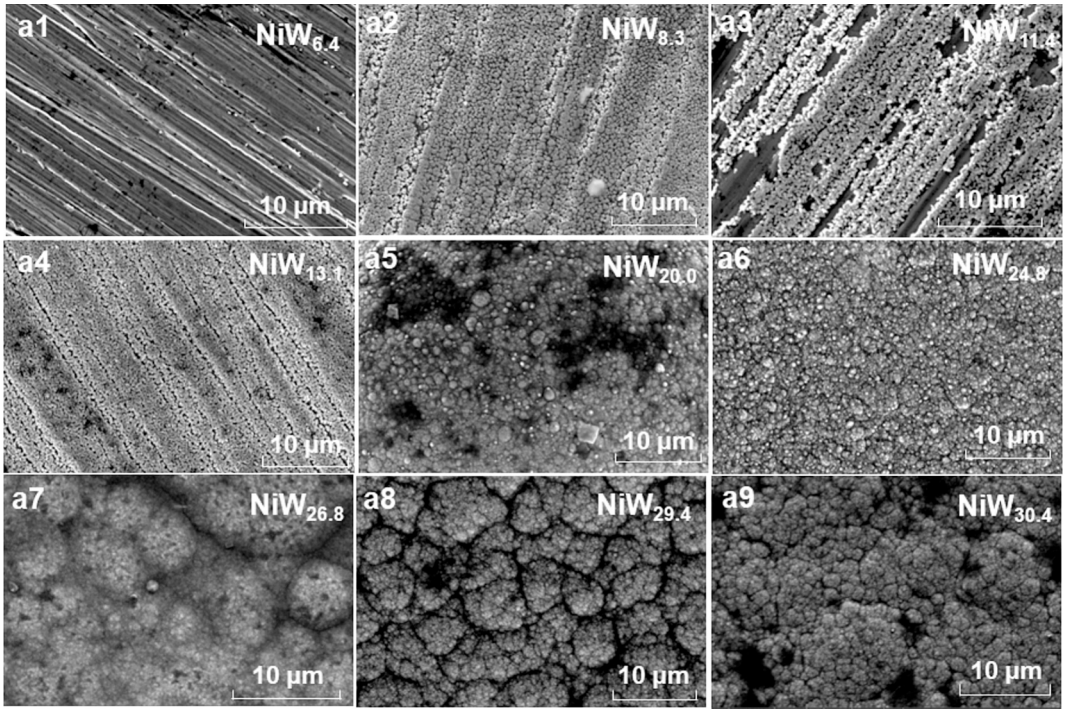

Fig. 3. SEM images of NiW electrodeposited alloy coatings with variation W content from 6.4 wt% to 30.4 wt%.

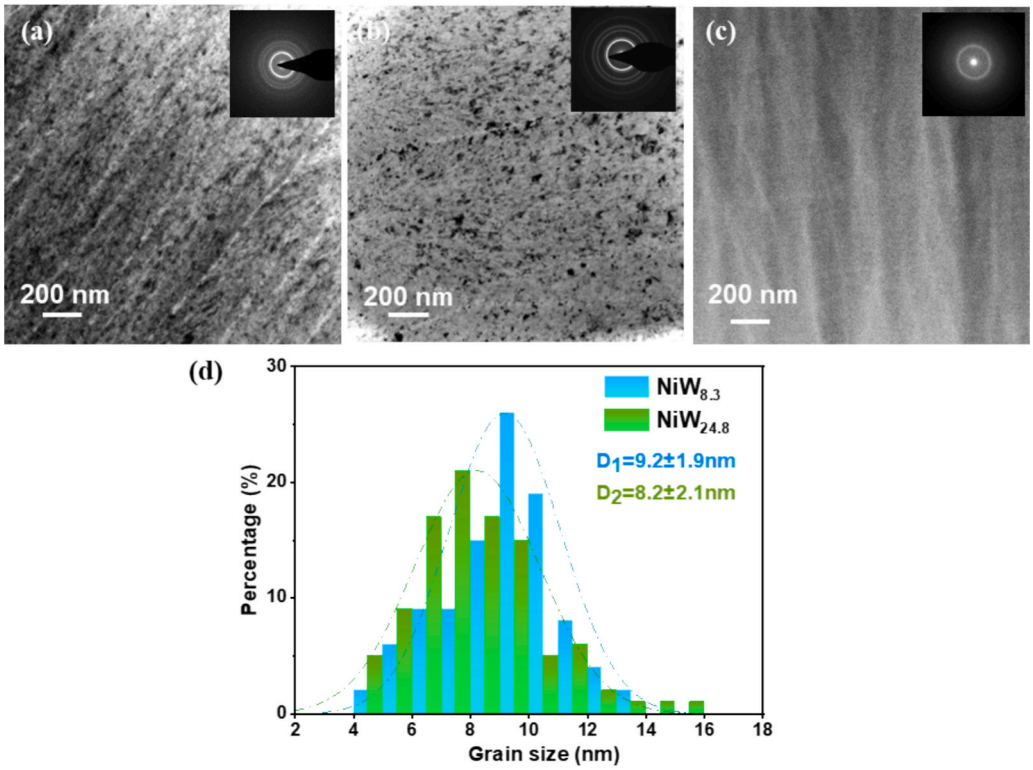

Fig. 4. TEM images of NiW coatings with W content of 8.3 wt% (a), 24.8 wt% (b) and amorphous (c) and grain size distribution images (d).

excellent conductivity and are used as anodes in electrodeposition processes. During the electroplating process, the anode is inevitably consumed. The loss of graphite anode is highly probable to trigger that graphite particles transfer into electrodeposition solution medium. When particles are present in medium, they will further co-deposit with ions or complexes to form NiW composite coating on cathode substrate. The consumption of anodes in electrodeposition process is related to parameters such as time, temperature, etc., which directly affect the concentration of particles in the system. Graphite anode was used for preparing NiW coating instead of pure nickel anode. The formula of electrodeposition medium is consistent and NiW coatings were obtained again under the same conditions of time, temperature, and current density.

The surface morphology of NiW coatings obtained via graphite anode was shown in Fig. 5(a). The morphology consistent with original state of NiW alloy coating can be clearly observed in the image, with a certain number of GBs dispersed on the surface of NiW alloy. The ratio of the area occupied by GBs in the field of view to the total area is calculated to represent the co-deposition content of append particles. Fig. 5 presents the data in ascending order based on the proportion of GBs composition. The particle size of GBs typically ranges in the tens of micrometers. The size and quantity of composite fillers utilized are influential factors determining the performance variations among coatings. When the size of graphite composition is in the tens of micrometers range, exploring the amount of appended composite additives is the focus of research. Although GBs co-deposit with $NiCit^{-}$, WO_4^{2-} and $[NiCitWO_2]^{-}_{ads}$ on the cathode substrate (Sassi et al., 2012), the proportion of GBs in electrodeposition medium varies due to graphite anode consumption rate, so there is no correlation between the composite amount and the composition of NiW alloy. It is essential to explore the correlation between anode consumption and electrodeposition process. Furthermore, while varying W content leads to distinct surface morphologies in the initial NiW alloy coating, the distribution of GBs across different NiW alloys is random. Fig. 5(b1-b3) shows the SEM images of NiW-GBs surface morphology. The composite coatings at higher magnification revealed the presence of spherical micron sized GBs which dimension is consistent with OM images. GBs are randomly dispersed across the surface of the composite coating, with some embedded within the NiW coating, and they exhibit excellent compatibility with the surrounding structure. This observation indicates that the GBs released by the anode and successfully co-deposited with NiW. The EDS element distribution results of NiW-GBs coatings with different tungsten content are shown in Fig. S1. The results demonstrate that Ni and W is also uniformly distributed in the surface of NiW-GBs composite coating, and that carbon elements, i.e. GBs, are widely and randomly dispersed on the surface of composite coating. The degree of agglomeration is consistent with the particle morphology size characterized by SEM and OM. The cross-section SEM images and side view OM image of NiW-GBs coatings are shown in Figs. S2 and S3, micro sized GBs are encapsulated in coatings or exposed on surfaces and due to local current density differences, the thickness of the sample edge as deposited is higher than the cross-sectional data at the center of coating. Overall, the results demonstrated that GBs were successfully incorporated into NiW coating without disrupting the uniform solid solution and the dispersion characteristics.

Fig. 5(c) and (d) additionally illustrates the fluctuation of W content in NiW-GBs composite coatings across various electrodeposition process parameters. The W content in NiW coatings fabricated through the ACCED method spans from 1.1 wt% to 35.5 wt%. In comparison to the original NiW alloy coating process, the W content of NiW-GBs produced via ACCED technology exhibits a similar trend with respect to temperature and current density. At 75 °C and 90 °C, the W content in alloys increases as the current density rises. However, at 60 °C, no such relationship is observed. Interestingly, transitioning the anode material from pure nickel to graphite exhibits minimal impact on the compositional variations within NiW alloy. The relationship between the proportion of GBs in NiW-GBs composite coatings and various process parameters is illustrated in Fig. 5(e). As the current density and temperature increase in ACCED process, the proportion rises (from 0.86 % to 3.93 %). This suggests that harsher conditions facilitate the release of

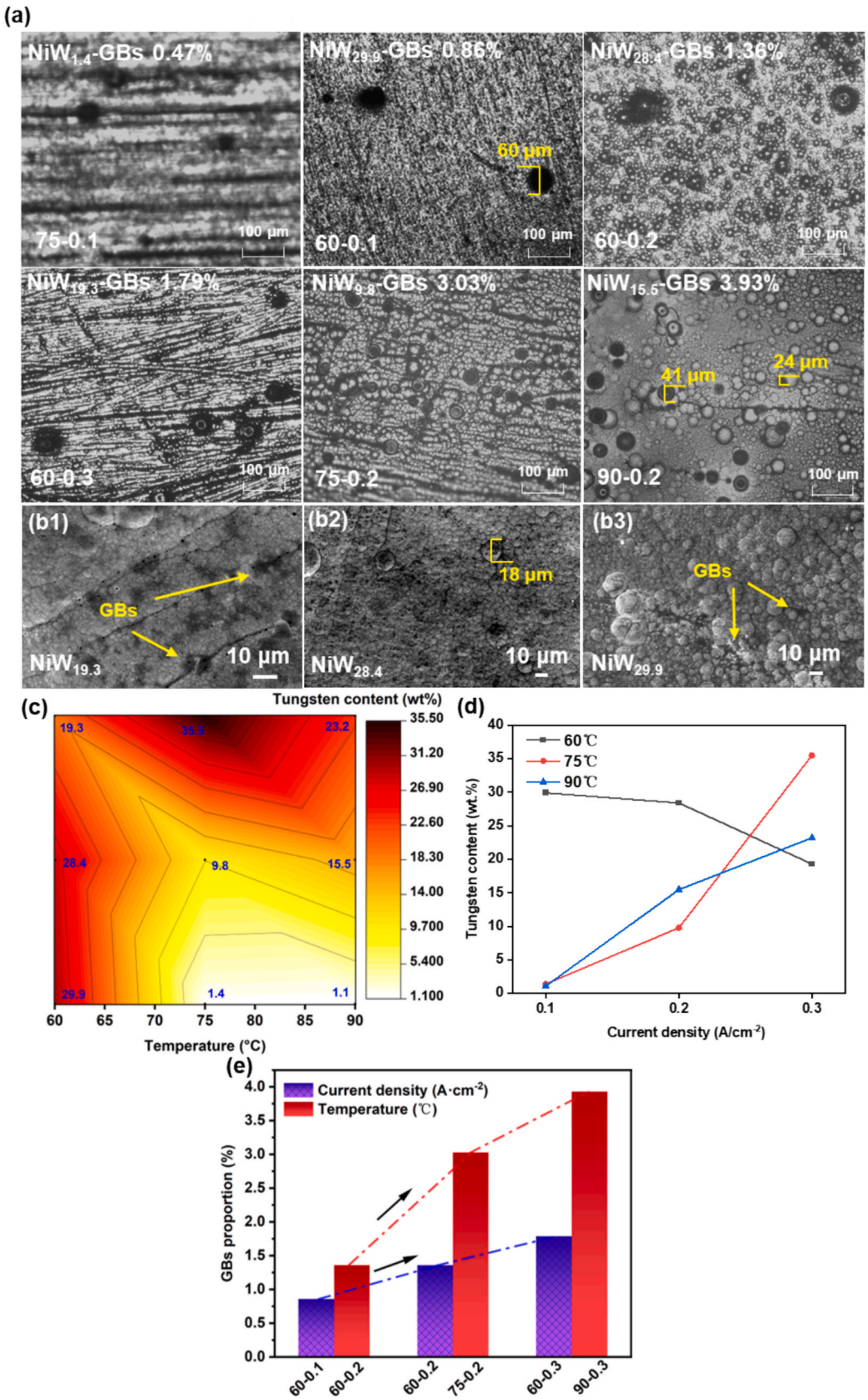

Fig. 5. Optical microscope images of NiW-GBs composite coatings via ACCED technic under various composition proportion and deposition parameters (temperature-current density) (a), SEM images of NiW-GBs (b1-b3), distribution mapping and relationship of W content with temperature and current density in ACCED technic (c) and (d), the relationship of GBs proportion and temperature or current density (e).

GBs from the graphite anode into the system and elucidates the co-deposition synthesis mechanism of NiW-GBs coatings.

3.2.2. XRD characterization of NiW-GBs coatings

XRD diffractograms of NiW-GBs electrodeposited coatings via ACCED are shown in Fig. 6. The results of XRD curves are arranged and displayed according to the amount of W content. All these coatings exhibit peaks at 44.5° represent the γ-Ni, this inference is consistent with the ICDD data base of the face centered cubic Ni (PDF # 04-0850) as references. Normally, the Ni–W alloy films grow along (111) direction as minimization of surface energy is favored. The grain sizes were determined by applying the Scherrer formula for XRD peak broadening to the (111) reflections and were marked on all samples (Giga et al., 2006). (111) peaks' width increases with the rise in W content, while the grain size shows a gradual decreasing trend simultaneously. After the W content exceeds 35.5 wt%, the grain size decreases to a minimum of 1.98 nm and the (111) peak of NiW gradually transforms into an amorphous peak, indicating the disappearance of nanocrystalline. Additionally, the shift of peaks from Ni-W with high W content toward lower angles, in comparison with thin Ni coatings, may be attributed to the formation of tungsten solid solution in FCC nickel (α-Ni(W)) (Allahyarzadeh et al., 2016). Increasing the W content in NiW coatings is widely acknowledged to have a refining effect on grain size (Hasegawa et al., 2017; Huang et al., 2021; Munagala et al., 2023). Nevertheless, the trend of grain size transition from nanocrystalline to amorphous as the W content varies has not been entirely clarified for materials spanning from pure Ni to Ni-rich and W-rich NiW coatings. In fact, calculations show that when the grain size is less than 2 nm, nanocrystals will transform into amorphous.

The grain size of NiW-GBs composite coatings was calculated and compared to that of NiW with similar W content to verify the effect of GBs co-deposition on grain nucleation. The grain size of $NiW_{9.8}$ and $NiW_{19.3}$ are 7.2 nm and 4.2 nm, respectively. The co-deposition of carbon particles creates active sites for NiW nucleation (Yu et al., 2022; Yu et al., 2024), inhibits grain agglomeration, and the pinning at grain boundaries restricts their expansion, thereby refining the grains (Chen et al., 2021). According to the Hall-Petch relationship, the ACCED process with GBs contributes to achieving higher strength (Ong et al., 2019).

3.3. Hardness

3.3.1. Hardness of NiW coatings

Surface hardness of NiW coating is an important mechanical property in applications as shown in Fig. 7, pure nickel and nickel-based alloy coatings are widely used due to their high initial hardness (Bigos et al., 2021; Wasekar et al., 2016; Lin et al., 2018). The hardness of pure nickel coating is 540HV from our previous work (Liu et al., 2024). After W atoms are solid dissolved in nickel, the hardness slightly increases and continues to harden with the overall W content of the coating. This is related to the monotonic range of solid solution strengthening and grain size variation in the Hall-Petch enhancement (Borgia et al., 2011). This change approximately develops in a linear relationship. In the direct current electroplating preparation of NiW coatings involved in present work, the highest W content reached 30.4 wt%, and its hardness reached 795HV. The linear regression of this relationship quantifies the contribution of W content to hardening, with the slope of the line representing the change in hardness corresponding to an increase in W content being approximately 7.3. Although this involves the transformation of nanocrystalline and amorphous in NiW coatings or the refinement of grain size, the relationship between W content and hardness indicates still continuous hardening, which does not affect the subsequent discussion (Yu et al., 2025). This provides empirical support for the contributions of solid solution effects and composite enhancement strengthening, respectively.

3.3.2. Hardness of NiW-GBs coatings via ACCED

The surface hardness of NiW-GBs composite coating prepared by ACCED varies with W content as shown in Fig. 8. Overall, the hardness of the composite coating ranges between 608 and 853 HV, significantly higher than that of the original NiW coating. The surface hardness of the composite coating shows an overall upward trend with increasing W content, which is consistent with the NiW electrodeposited coating. This clear positive correlation is evident in the low W solid solution region, and in the amorphous region with high W content towards the end of the curve. The middle part of the curve is affected by the composite effect of GBs, which changes the relationship between hardness and the increase of W content, that is, the decrease of grain size. This change is caused by the addition of various amounts of GBs due to the ACCED technology. The microstructural parameters and surface hardness of the NiW-GBs coatings are listed in Table 2.

For the wear resistance of NiW and NiW-GBs coatings at the same electrodeposited parameters (75 °C–0.2 A/cm^{-2}) and with similar W

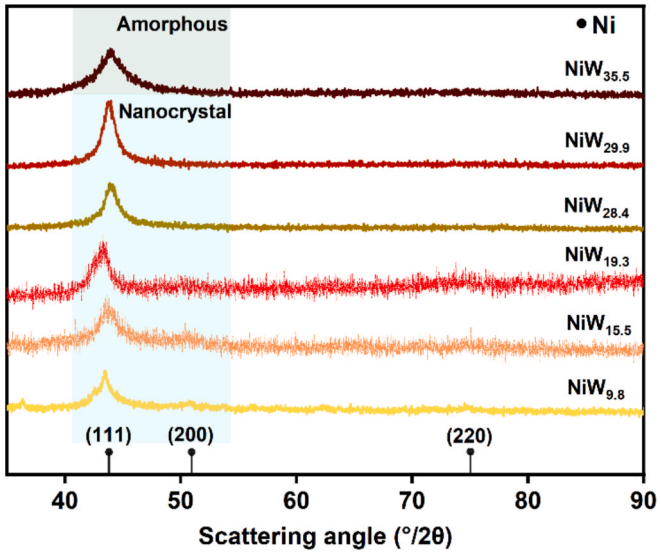

Fig. 6. XRD spectra of wide W content NiW-GBs composite coatings via ACCED technology.

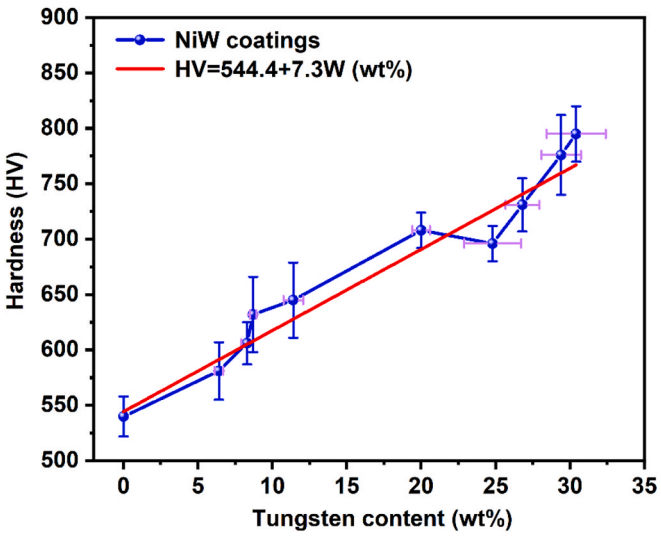

Fig. 7. Relationship of hardness and W content of NiW electrodeposited coatings.

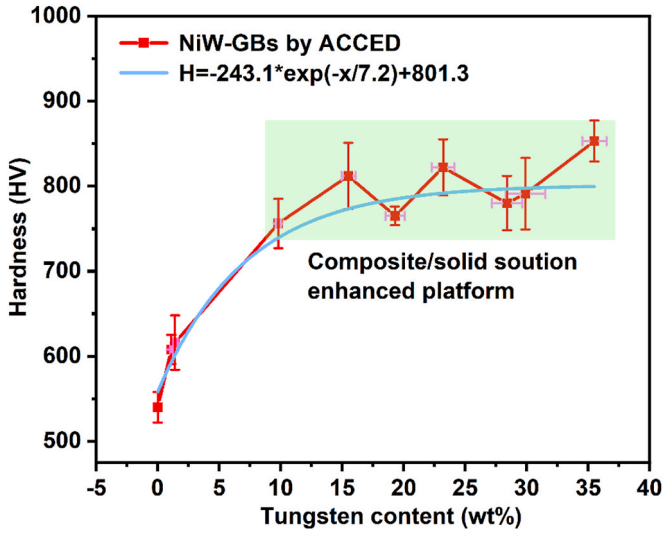

Fig. 8. Relationship of hardness and W content of NiW-GBs coatings by ACCED.

Table 2
Structure parameters of NiW-GBs coatings.

No.	Electrodeposition parameters	W content (wt%)	GBs proportion (%)	Grain size (nm)	Hardness (HV)
1	75 °C 0.1 A/cm^2	1.4	0.47	11.18	616
2	75 °C 0.2 A/cm^2	9.8	3.03	7.05	756
3	90 °C 0.2 A/cm^2	15.5	3.93	5.65	812
4	60 °C 0.3 A/cm^2	19.3	1.79	7.13	765
5	60 °C 0.2 A/cm^2 A/cm^2	28.4	1.36	3.62	780
6	60 °C 0.1 A/cm^2	29.9	0.86	4.70	791

content as shown in Fig. S4. The average friction coefficient (COF) was decreased from 0.84 to 0.33 after co-deposited with GBs (3.03 %) by ACCED. Furthermore, the wear rate reduced by 72.6 % as the hardening and lubrication of GBs, indicating the comprehensive improvement of wear resistance during ACCED.

3.4. Thermal stability of NiW and NiW-GBs coatings

The variations of hardness of NiW and NiW-GBs by ACCED with increasing annealing time at 400, 600 and 800 °C are shown in Fig. 9(a), (b) and (c). For annealing at 400 °C, the hardness of the NiW coatings first increases with increasing annealing duration up to 60 mins and then slightly decreases for longer annealing durations. By contrast, the hardness values for the NiW-GBs monotonically increase to 1236 HV with increasing annealing duration at 400 °C to 120 mins. This annealing hardening phenomenon can be attributed to the grain boundary relaxation of nanocrystals present on the coating (Detor and Schuh, 2007). The difference in thermal stability attributed to GBs arises from the diffusion effects of particles and their pinning at NiW grain boundaries, which restricts their movement (Chen et al., 2021; Hosseini et al., 2014). For annealing temperature at 600 °C, the hardnesses of both the NiW and NiW-GBs exhibit consistent increments within 1 h, in line with other studies (de Lima-Neto et al., 2010; Auerswald and Fecht, 2010; Khan et al., 2011); and minor decrements as the annealing duration extending to 2 h. When the annealing temperature is ascended to 800 °C, the hardness of NiW coating gradually diminishes with prolongated annealing time, attributed to the significant growth of nanocrystals. Specifically, the pure NiW coating reached its lowest hardness at 533 HV after 0.5 h, while the hardness of NiW-GBs stabilizes after 1 h. This is contributed to the effectively suppress grain coarsening and hinder diffusion from GBs composition.

The relationship between hardness and annealing temperature during 1 h and 2 h annealing durations is illustrated in Fig. 9(d) and (e). The hardness of coatings initially rises and then falls with increasing annealing temperature to 800 °C. For 1 h annealing, the peak hardness of the NiW coating is achieved at 400 °C, while hardness of the NiW-GBs coating further increases after annealing at 600 °C. When the annealed time is extended to 2 h, the peak hardness was achieved at 400 °C for both of coatings. The softening phenomenon after peak hardness is caused by grain growth during long-term annealing at high temperatures, consistent with the results of isothermal heat treatment. After annealing at 800 °C, both types of coatings exhibit lower hardness than those at the as-deposited state. The above results are consistent with previous literature reports, except that softening caused by prolonged annealing at 600 °C to 2 h is rarely reported (Huang et al., 2021; Khan et al., 2011).

Overall, the NiW-GBs composite coatings have greater initial hardness, stronger annealing hardening effect, and better thermal stability compared to the NiW alloy coating, indicating that the graphite fillers play a significant role in strengthening the NiW alloy and enhancing thermal stability.

4. Disscussion

4.1. Hardening of GBs composition

Hardness is a base parameter of materials reflects the surface stress and strength. The hardness of NiW and NiW-GBs by ACCED technology specimens is shown in Fig. 10(a). The hardness of NiW alloy coatings, fabricated by nickel and graphite anodes respectively, rises with the escalation of W content. Within the framework of ACCED technology, when the W content reaches 35.5 wt%, the hardness of the coating elevates from 540 HV for pure nickel to 853 HV. Similarly, the hardness of original Ni-30.4 wt% W also improves to 795 HV. NiW alloy employs nickel as the solvent and tungsten atoms as the solute. Structurally, tungsten occupies the lattice sites of nickel to create FCC substitution solid solution. As the tungsten content in the deposition layer increases, the lattice distortion increases, indicating a greater resistance during dislocation movement in the alloy structure. Consequently, the hardness of NiW alloy increases. In comparison to NiW alloys prepared via nickel anode, NiW-GBs composite coatings fabricated through ACCED technology exhibit higher hardness, demonstrating the incorporating graphite balls composition enhanced NiW alloys from graphite anode consumption.

To further investigate the mechanism of ACCED technology, interpolation extrapolation method was employed to calculate the hardening rate and explored the relationship with a broad spectrum of W content as shown in Fig. 10 (a). The method for calculating the hardening rate (η) is presented in Eq. (1).

$$\eta = \frac{H_{comp} - H_{ori}}{H_{ori}} \times 100\% \quad (1)$$

Here, H_{ori} and H_{comp} represent the hardness of NiW as deposited and NiW-GBs prepared via ACCED, respectively. Linear interpolation facilitates continuous correspondence between the hardness and W content of NiW and NiW-GBs coatings, thereby enabling a more effective calculation of the hardening rate via the deviation of function value. The average hardening rate of the majority of composite coatings through ACCED technology remains around 10 %-20 %. For NiW alloys containing 9.8 % and 15.5 wt% W, the respective maximum hardening rates can reach 18.63 % and 20.29 % which are marked as A and B. Additionally, two NiW-GBs composite coatings with high W contents of 28.4 wt% and 29.9 wt% were selected and designated as C and D for the analysis of the dual factors of graphite proportion and W content affecting the hardness strengthening rate. Overall, there appears to be no direct correlation between hardening rate and variations in W content,

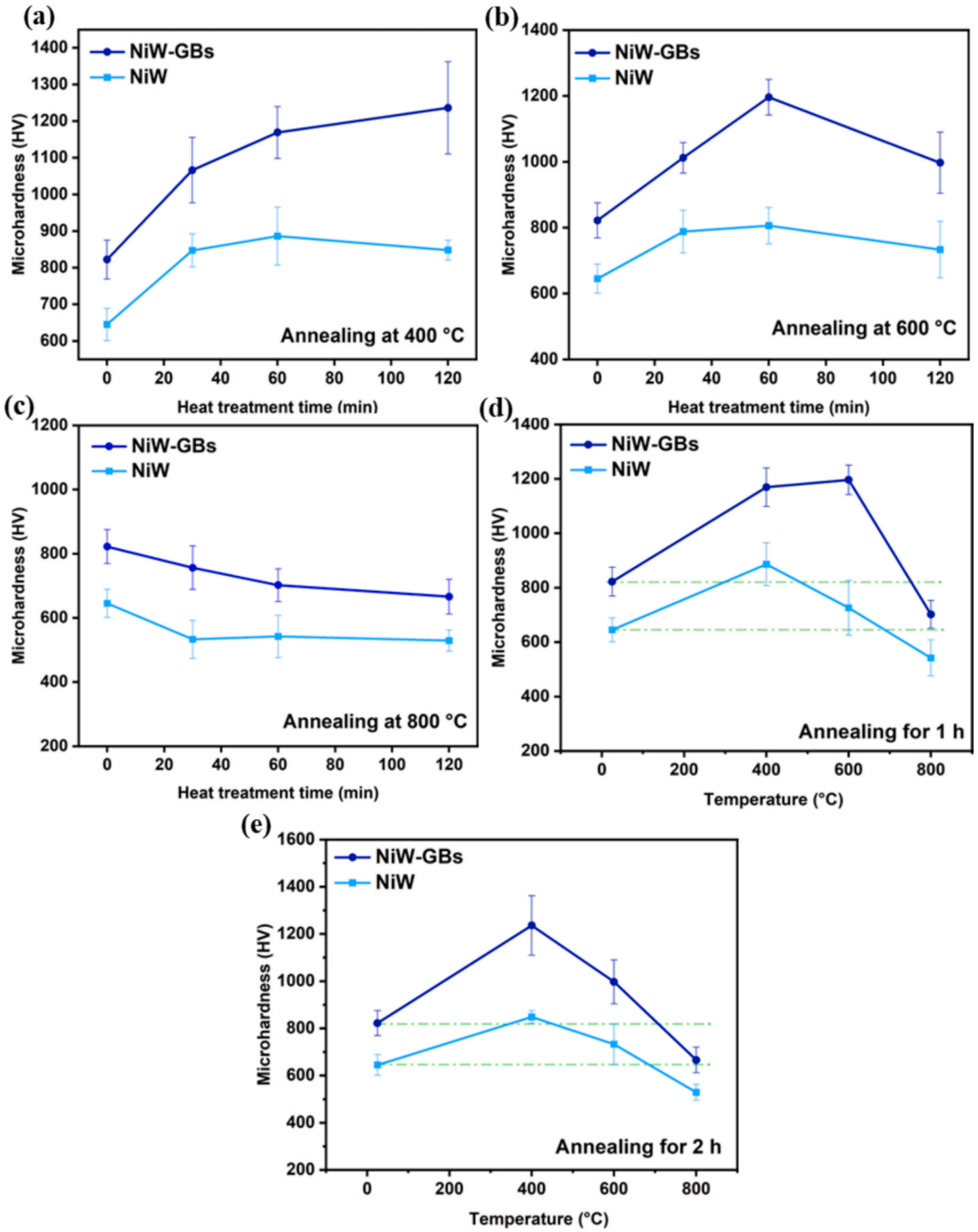

Fig. 9. Relationship between hardness of NiW and composite coatings and duration of annealing at specified temperature (a) 400 °C, (b) 600 °C, (c) 800 °C or specified period (d) 1 h and (e) 2 h.

suggesting that the vanishing of the anode and the recombination of graphite are not directly related to the W deposition process. In Fig. 10 (b), the correlation mapping between hardening rate and electrodeposition parameters reveal that NiW-GBs coatings exhibiting higher hardening rate were prepared through a preparation process involving high current density or elevated temperature zones. It indicates that graphite anode consumption and graphite balls doping are more likely to take place under specific process condition. The course of ACCED technology entails the initial consumption of the anode at high temperatures, followed by the concurrent adsorption of GBs with a high cathode charge attraction and the co-deposition with NiW coating.

Fig. 10(c) illustrates the relationship between the hardening rate of NiW alloy coating by graphite balls and the fillers proportion. The fitting equation for relationship curve is displayed in Fig. 10(d). For NiW-GBs composite coating prepared via ACCED technology, the proportion of composite fillers ranges from 0 % to 4 %. Within this range, the hardening rate of graphite balls on NiW alloy coatings increases monotonically as the proportion rises. The progression of this relationship is

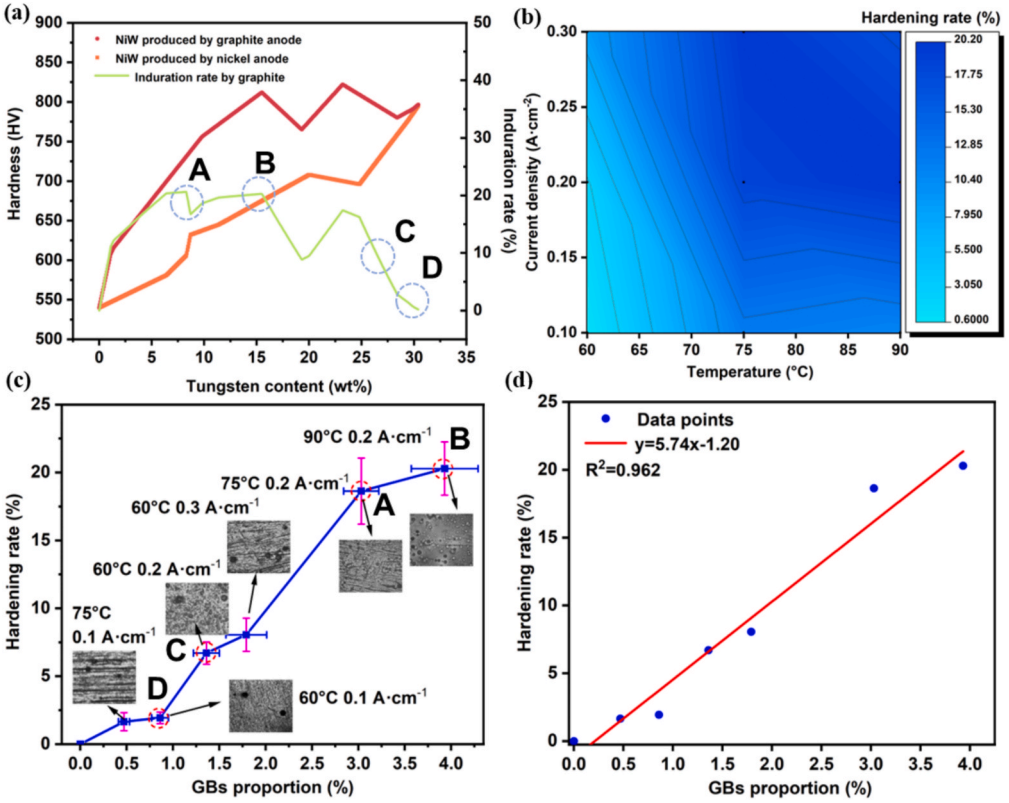

Fig. 10. Relationship between hardness of either NiW or NiW-GBs electrodeposited coatings and tungsten content (a), mapping of hardening rate and electrodeposition parameter (b), relationship between hardening rate and GBs proportion (c) and its fit curve (d).

influenced by hidden factors associated with the process parameters of electrodeposition, as illustrated in Fig. 10(c). At a medium temperature of 60 °C, a slight increase in the current density results in a minor rise in the proportion of composite graphite balls. However, when the system temperature reaches 75 °C and 90 °C, the proportion of filler particles exhibits exponential growth (elevating from 1.36 % to 3.03 % and 3.93 % respectively), consequently leading to a rapid increase in the hardening rate (escalating from 6.70 % to 18.63 % and 20.29 %). This suggests that excessively high temperatures during the electrodeposition process are advantageous for anode consumption and composite co-deposition. The linearly increasing relationship depicted in the fitting results suggests that the ACCED process generates a positive feedback effect on the hardening process by integrating graphite balls into coating.

4.2. Strengthening mechanisms

The hardness of a given composite alloy material can be represented as the sum of contributions from the hardening mechanisms that it exhibits. Here, the NiW and NiW-GBs coatings is free of microcracks demonstrating well compactness as shown in Figs. 3 and 5. And the micro-scale GBs show excellent interface bonding and composite compatibility with the NiW matrix in horizontal and vertical directions (Figs. S2 and S3), respectively. Hence, although the interface bonding between GBs and NiW matrix impacts on the hardening effect, it can be ignored under enough splendid composite compatibility. So, one of the simplest formulations of this is:

$$H = H_{SS} + H_{CE} \tag{2}$$

where H_{SS} is solid-solution (SS) hardening and H_{CE} is composite enhance. The partial factors of H_{SS} were determined by fitting the relationship curve between hardness and W content in NiW alloy. Consequently, it is essential to fit the relationship between hardness and the addition of graphite balls after removing the H_{SS} factors to ascertain the H_{CE} component which result is shown in Fig. 11. Logistic model effectively describes the relationship between the variables. When the proportion of GBs fillers ranges from 1.5 % to 3.0 %, the enhancement effect significantly improves as the proportion increases.

Consequently, the description of H can be articulated more precisely, as demonstrated in Eq. (3). The initial segment of the equation illustrates the strengthening of W solid solution embedded in FCC nickel, while the latter segment represents the enhancement provided by composite particles composed of GBs via ACCED.

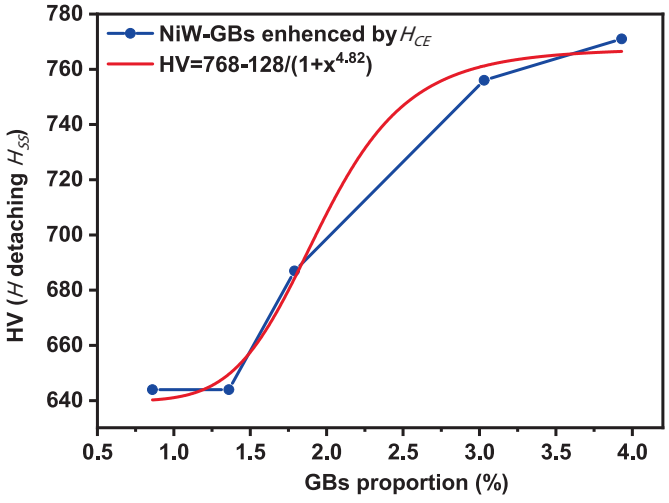

Fig. 11. Relationship of hardness (H detaching H_{SS}) and GBs proportion and its logistic model.

$$H = (544.4 + 7.3Wwt.\%) + [768.0 - \frac{128}{1 + P_{GBs}{}^{4.82}}] \quad (3)$$

where P_{GBs} represents the proportion of GBs co-electro-deposited. The W content influences the strengthening mechanism through either solid solution formation or grain size refinement, establishing a continuous enhancement relationship. However, the doping of GBs imposes a limit on the hardening of NiW upper limit value to 768.0HV at 3.9 % for P_{GBs}. A moderate amount of composite hardening effect is particularly significant.

4.3. Comparison of NiW-GBs and other NiW electrodeposited coatings

Current research indicates that the incorporation of reinforcing phase particles significantly enhances the surface hardness of coatings. Nonetheless, variations in the types, sizes, and quantities of these particles lead to differing properties. Fig. 12(a) illustrates a comparison of hardness and hardening rates of Ni-based or NiW-based composite coatings prepared by traditional composite deposition from existing literature. However, for the ACCED technology, there is no step to introduce any additional composite particles or chemicals into the electrodeposited solution. The NiW-GBs composite coating can be produced by continuously releasing graphite balls into the medium through the consumption of the anode and co-depositing them at the cathode. NiW coatings as deposited prepared present work exhibits high initial hardness. The incorporation of inorganic nonmetallic particles as the second phase significantly enhances the coating's strength. Compared to carbon materials, ceramic particles demonstrate a more pronounced increase in hardness, likely due to the comparatively lower initial hardness or higher doping concentration of the composite fillers. Consequently, the strength of the second-phase particles emerges as the primary factor influencing hardness in the test. When diamond or graphite particles are used as the dopants, the hardness of NiW composite coating can exceed 800 HV, with acknowledgment of the assistance from the original excellent hardness. Additionally, annealing following the addition of second-phase particles further elevates the coating hardness. Thereinto, NiW-GBs coatings via ACCED technology exhibit the most remarkable hardening rates at 81.2 % and 85.4 %, respectively, showcasing the favorable impact of carbon materials on enhancing thermal stability. What's more, NiW and diamond composite coatings achieve the most outstanding after annealing at 600 °C for 1 h, surpassing 1250 HV. Overall, NiW alloy coating initially prepared in this study exhibited high initial hardness. The graphite particles chosen display a remarkable rate of performance enhancement in carbon materials, comparable to hard particles like SiO_2, BN. This enhancement arises from the synergy between the inherent physical properties of carbon materials and their unique structure that aids in grain size reduction. Subsequent annealing treatment further boosts the hardness of the composite coating, signifying commendable thermal stability. The ACCED technic substantially enhances the hardness and thermal stability of NiW-GBs composite coatings, offering significant benefits by

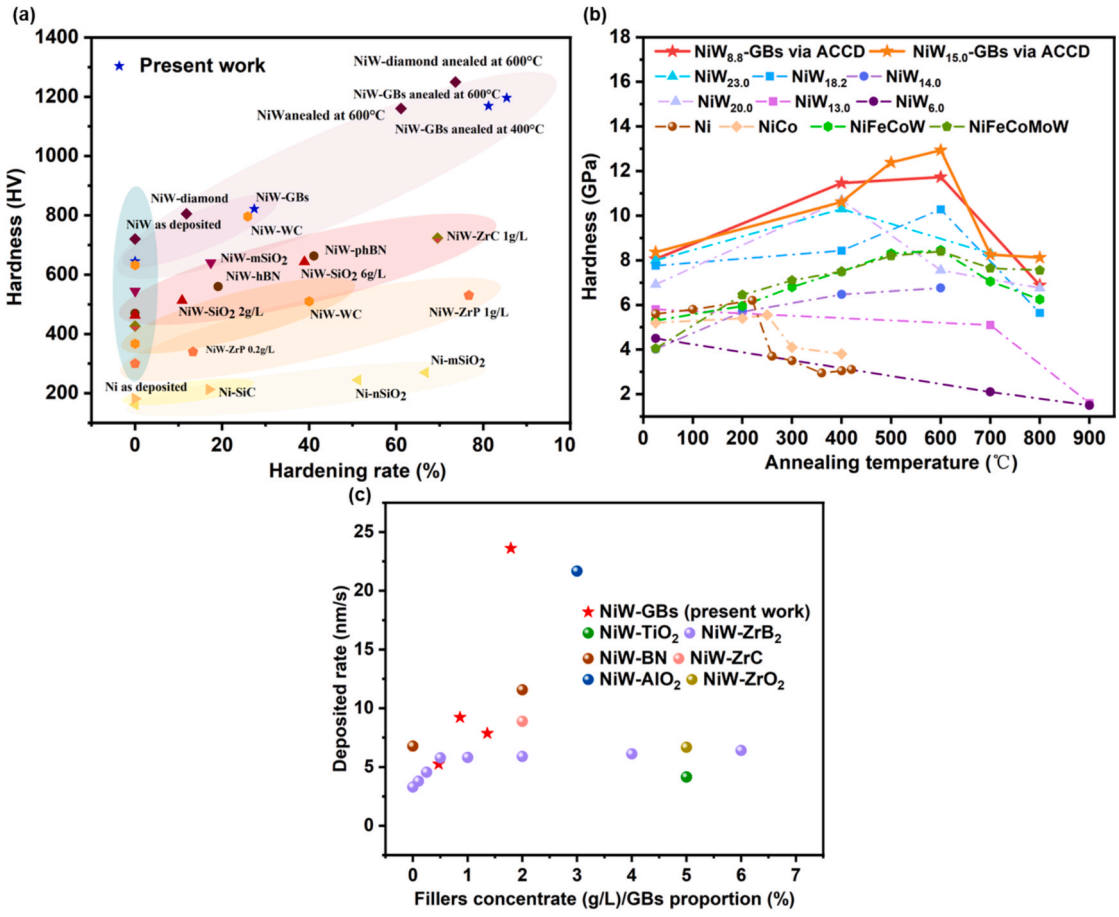

Fig. 12. (a) Hardness and hardening rate of Ni, NiW and composite coatings with SiO_2 (Xijing and Yong, 2023; Liao et al., 2022; Lekka et al., 2012), BN (Cheng et al., 2024), diamond (Wang et al., 2014); SiC (Nayak et al., 2024), WC (Boonyongmaneerat et al., 2010); ZrC (Li et al., 2021) and ZrP (Li et al., 2021). (b) Hardness and thermal stability of NiW-GBs via ACCED as compared to nickel-based materials Ni (Torrents et al., 2010); NiCo (Kong et al., 2022); NiFeCoW and NiFeCoMoW (Hache et al., 2024); NiW alloys with 6.0 at.% and 13.0 at.% (Sunwang et al., 2011), 20.0 at% (Schlossmacher and Yamasaki, 2000); 14.0 at.% (de Lima-Neto et al., 2010); 18.2 at.% (Huang et al., 2021); 23.0 at.% (Marvel et al., 2016). (c) Deposited rate of NiW-GBs via ACCED and NiW-TiO_2 (Li et al., 2024), NiW-ZrB_2 (Li et al., 2022); NiW-BN (Cheng et al., 2024); NiW-ZrC (Li et al., 2021), NiW-Al_2O_3 (Kumar et al., 2024), NiW-ZrO_2 (Beltowska-Lehman et al., 2020).

streamlining the process and reducing material usage.

For the mechanical performance and thermal stability of Ni and Ni-based alloy, an overall comparison between NiW-GBs via ACCED and other materials is shown in Fig. 12(b). Each of these exemplars was initially fabricated with a homogeneous nanocrystalline structure and subsequently annealed for 1 h at varying temperatures to investigate the thermal stability of grain size and hardness. The softening critical temperature due to grain growth in pure nickel is approximately 200 °C. When cobalt is added, this temperature increases by approximately 50 °C. The introduction of the refractory element W further elevates the critical temperature of grain growth to 400 °C. This enhancement occurs because pure tungsten possesses a higher intrinsic melting temperature (Hache et al., 2024). Additionally, with increased tungsten content or varying element types, the critical temperature may rise to around 600 °C. Notably, the NiW-GBs composition obtained via ACCED maintains a high critical temperature even at low tungsten content, with both the hardness and thermal stability remaining at elevated levels.

Deposited rate is an important parameter that determines production efficiency in engineering applications. The deposited rate values of NiW-GBs coatings were calculated via the sectional thickness (Fig. S2), and the corresponding values of other NiW composite coatings with present works were all shown in Fig. 12(c). For the composite coatings obtained by mild process parameters, the deposited rate is generally between 5 and 10 nm/s. While, for NiW-GBs, as increasing the temperature and current density to increase the proportion of GBs, the coating deposited rate is greatly improved, up to 23.6 nm/s, far more than traditional co-deposited processes. This indicates that ACCED technology has the advantages of controlling GBs release and rapid co-deposited.

5. Conclusion

In this study, ACCED technique was developed for the first time to facilitate the one-step appending graphite balls into NiW alloy coating which optimizes traditional co-deposition of composition coatings through a simplified operation and reduced the anode or fillers costs.

1. NiW alloy coatings with different W content from 0 wt% to 45.1 % were prepared via electrodeposition under various medium temperature from 60 °C to 90 °C and current density from 0.10 to 0.35 A/cm^2.
2. Micro-scale GBs are co-deposited with NiW alloy from a graphite anode using one-step electroplating technology to prepare NiW-GBs composite electrodeposited coatings.
3. Hardness and thermal stability of either NiW or NiW-GBs coatings prepared through ACCED was examined to elucidate the underlying mechanism, revealing that the hardness of NiW-GBs coating exceeds that of original NiW coating by up to 20.29 % under the action of pining and grain refinement.
4. The hardening rate under various W content was determined through interpolation extrapolation. The relationship between hardening rate and graphite proportion suggested that the composite GBs with NiW coating had a continuous enhancing effect on hardening via ACCED process particularly at high temperature or current density.
5. The contributions of increased W content and the addition of varying amounts of GBs to strengthening are calculated and analyzed separately to elucidate the reinforcement mechanism.

CRediT authorship contribution statement

Zhifei Yu: Writing – original draft, Validation, Software, Methodology, Investigation, Formal analysis. **Xingwen Zhang:** Investigation, Formal analysis. **Zhan Liu:** Methodology, Investigation. **Shaojia Shi:** Methodology, Investigation. **Qingzhong Mao:** Data curation, Conceptualization. **Yonghao Zhao:** Writing – review & editing, Supervision, Funding acquisition, Conceptualization. **Zesheng You:** Writing – review & editing, Visualization, Conceptualization.

Declaration of competing interest

The authors declare that they have no known competing financial interests or personal relationships that could have appeared to influence the work reported in this paper.

Acknowledgements

Y.H. Zhao acknowledges financial supports from the National Key R&D Program of China (Grant No. 2021YFA1200203), National Natural Science Foundation of China (Grant No. 51971112 and 51225102) and Jiangsu Province Leading Edge Technology Basic Research Major Project (BK20222014) and the Fundamental Research Funds for the Central Universities (Grant No. 30919011405). The authors also want to acknowledge the support of the Jiangsu Key Laboratory of Advanced Micro-Nano Materials and Technology. SEM, TEM and EBSD experiments are performed at the Materials Characterization and Research Center of Nanjing University of Science and Technology.

Appendix A. Supplementary data

Supplementary data to this article can be found online at https://doi.org/10.1016/j.ces.2025.122402.

Data availability

Data will be made available on request.

References

Figuet, D., Billard, A., Savall, C., Creus, J., Cohendoz, S., Grosseau-Poussard, J.L., 2022. A comparison between the microstructure and the functional properties of NiW coatings produced by magnetron sputtering and electrodeposition. Mater. Chem. Phys. 276. https://doi.org/10.1016/j.matchemphys.2021.125332.

Dash, P., Panda, P.K., 2024. Top-down Strategies Synthesis of 2D Nanomaterial. 2D Nanomater. 1–16.

Geng, X., Liu, F., Gan, J., Si, Z., Zhang, R., 2023. Interface failure analysis of coating in gun barrel under thermal-pressure coupling effect. J. Phys. Conf. Ser. 2478 (12), 122019. https://doi.org/10.1088/1742-6596/2478/12/122019.

Liao, X.B., Zhou, R.B., Yang, Y.F., Gong, C.H., 2014. Study on the erosion and abrasion mechanism of the modern artillery barrel. Res. Mech. Eng. Mater. Sci. 456, 433–437. https://doi.org/10.4028/www.scientific.net/AMM.456.433.

Sieber, M., Scharf, I., Herold, F., Schmidt, A., Böttger, D., Böttger, S., Böttger, E., Götze, U., Lampke, T., 2016. Anodic oxidation of AlMgSi1 — Coatings' mechanical properties, process costs and energy consumption of the oxide formation. Mater. Des. 89, 1259–1269. https://doi.org/10.1016/j.matdes.2015.10.064.

Pierre, F., Diebold, F., Baruthio, F., 2008. Biomonitoring of two types of chromium exposure in an electroplating shop. Int. Arch. Occup. Environ. Health 81 (3), 321–329. https://doi.org/10.1007/s00420-007-0216-x.

Saravanan, G., Mohan, S., 2009. Corrosion behavior of Cr electrodeposited from Cr(VI) and Cr(III)-baths using direct (DCD) and pulse electrodeposition (PED) techniques. Corros. Sci. 51 (1), 197–202. https://doi.org/10.1016/j.corsci.2008.10.005.

Klement, U., da Silva, M., Hibbard, G.D., 2009. Thermal stability in nanocrystalline electrodeposits - a comparison of Ni- and Co-based materials. Nanostruct. Metals: Fundament. Appl. 231–238.

Hasegawa, M., Guillonneau, G., Maeder, X., Mohanty, G., Wehrs, J., Michler, J., Philippe, L., 2017. Electrodeposition of dilute Ni-W alloy with enhanced thermal stability: Accessing nanotwinned to nanocrystalline microstructures. Mater. Today Commun. 12, 63–71. https://doi.org/10.1016/j.mtcomm.2017.06.002.

Detor, A.J., Schuh, C.A., 2007. Tailoring and patterning the grain size of nanocrystalline alloys. Acta Mater. 55 (1), 371–379. https://doi.org/10.1016/j.actamat.2006.08.032.

Schuh, C.A., Nieh, T.G., Iwasaki, H., 2003. The effect of solid solution W additions on the mechanical properties of nanocrystalline Ni. Acta Mater. 51 (2), 431–443. https://doi.org/10.1016/S1359-6454(02)00427-5.

Low, C.T.J., Wills, R.G.A., Walsh, F.C., 2006. Electrodeposition of composite coatings containing nanoparticles in a metal deposit. Surf. Coat. Technol. 201 (1–2), 371–383. https://doi.org/10.1016/j.surfcoat.2005.11.123.

Cheng, X., He, Y., Fan, Y., Yan, L., Zhou, H., Zhong, J., Li, Z., Song, J., 2024. Strengthening the mechanical properties and corrosion resistance of Ni W coatings by PDA-functionalized h-BN nanosheets. Diam. Relat. Mater. 141. https://doi.org/10.1016/j.diamond.2023.110567.

Xijing, L., Yong, C., 2023. Effect of SiO2 nanoparticles on the hardness and corrosion resistance of NiW/SiO2 nano composite coating prepared by electrodeposition. Int. J. Electrochem. Sci. 18 (6). https://doi.org/10.1016/j.ijoes.2023.100138.
Wang, H.T., Sheu, H.H., Ger, M.D., Hou, K.H., 2014. The effect of heat treatment on the microstructure and mechanical properties of electrodeposited nanocrystalline Ni-W/diamond composite coatings. Surf. Coat. Technol. 259, 268–273. https://doi.org/10.1016/j.surfcoat.2014.03.064.
Liao, Z.Q., Zhong, F.P., Zhang, Z.Q., Jiang, L., Wei, G.Y., Yuan, M., Ren, L.L., 2022. Comparative study on the wear resistance and corrosion resistance of NiW and NiCoW composite coatings with micro- and nano-SiC particles. Mater. Today Commun. 33. https://doi.org/10.1016/j.mtcomm.2022.104769.
Lanzutti, A., Lekka, M., de Leitenburg, C., Fedrizzi, L., 2019. Effect of pulse current on wear behavior of Ni matrix micro-and nano-SiC composite coatings at room and elevated temperature. Tribol. Int. 132, 50–61. https://doi.org/10.1016/j.triboint.2018.12.011.
Lekka, M., Lanzutti, A., Casagrande, A., de Leitenburg, C., Sonora, P.L., Fedrizzi, L., 2012. Room and high temperature wear behaviour of Ni matrix micro- and nano-SiC composite electrodeposits. Surf. Coat. Technol. 206 (17), 3658–3665. https://doi.org/10.1016/j.surfcoat.2012.03.016.
Uysal, M., Algül, H., Duru, E., Kahraman, Y., Alp, A., Akbulut, H., 2021. Tribological properties of Ni-W-TiO-GO composites produced by ultrasonically-assisted pulse electro co-deposition. Surface Coat. Technol. 410. https://doi.org/10.1016/j.surfcoat.2021.126942.
Chen, Z.M., Tan, H., Jin, K.J., Cheng, J., Zhu, S.Y., Zhang, B.W., Yang, J., 2025. Microstructure and high temperature tribological properties of copper-based graphite composite coatings reinforced with in-situ Fe3C. Tribol. Int. 204. https://doi.org/10.1016/j.triboint.2024.110452.
Ren, S.H., Xia, X.C., Song, K.H., Ding, J., Geng, K.P., Song, G.X., Huo, C.X., Wang, Y.J., Liao, W.D., Hua, N.X., Chen, X.G., 2025. Effect of adding copper-plated graphite on the organization and wear reduction of Copper-Nickel alloy Composite Coatings. Surf. Coat. Technol. 496. https://doi.org/10.1016/j.surfcoat.2024.131661.
Su, J., Li, Y.Z., Duan, M.G., Liu, S.H., Liu, K., 2018. Investigation on particle strengthening effect in in-situ TiB/2024 composite by nanoindentation test. Mater. Sci. Eng. A-Struct. Mater. Properties Microstruct. Process. 727, 29–37. https://doi.org/10.1016/j.msea.2018.04.070.
Yamasaki, T., 2001. High-strength nanocrystalline Ni-W alloys produced by electrodeposition and their embrittlement behaviors during grain growth. Scr. Mater. 44 (8–9), 1497–1502. https://doi.org/10.1016/S1359-6462(01)00720-5.
Somekawa, H., Nieh, T.G., Higashi, K., 2004. Instrumented indentation properties of electrodeposited Ni-W alloys with different microstructures. Scr. Mater. 50 (11), 1361–1365. https://doi.org/10.1016/j.scriptamat.2004.02.042.
Allahyarzadeh, M.H., Aliofkhazraei, M., Rezvanian, A.R., Torabinejad, V., Rouhaghdam, A.R.S., 2016. Ni-W electrodeposited coatings: Characterization, properties and applications. Surf. Coat. Technol. 307, 978–1010. https://doi.org/10.1016/j.surfcoat.2016.09.052.
Munagala, V.N.V., Wasekar, N.P., Bathini, L., Ramakrishna, L., Sundararajan, G., 2023. Deciphering the role of W content, triple junctions, and heat treatment on the corrosion performance of Ni–W alloy coatings used for automotive applications. Mater. Chem. Phys. 308, 128305. https://doi.org/10.1016/j.matchemphys.2023.128305.
Alimadadi, H., Ahmadi, M., Aliofkhazraei, M., Younesi, S.R., 2009. Corrosion properties of electrodeposited nanocrystalline and amorphous patterned Ni-W alloy. Mater. Des. 30 (4), 1356–1361. https://doi.org/10.1016/j.matdes.2008.06.036.
Eliaz, N., Sridhar, T.M., Gileadi, E., 2005. Synthesis and characterization of nickel tungsten alloys by electrodeposition. Electrochim. Acta 50 (14), 2893–2904. https://doi.org/10.1016/j.electacta.2004.11.038.
Mizushima, I., Tang, P.T., Hansen, H.N., Somers, M.A.J., 2005. Development of a new electroplating process for Ni-W alloy deposits. Electrochim. Acta 51 (5), 888–896. https://doi.org/10.1016/j.electacta.2005.04.050.
Schuh, C.A., Nieh, T.G., Yamasaki, T., 2002. Hall-Petch breakdown manifested in abrasive wear resistance of nanocrystalline nickel. Scripta Materialia 46 (10), 735–740. https://doi.org/10.1016/S1359-6462(02)00062-3 https://doi.org/Pii S1359-6462(02)00062-3.
Sriraman, K.R., Raman, S.G.S., Seshadri, S.K., 2006. Synthesis and evaluation of hardness and sliding wear resistance of electrodeposited nanocrystalline Ni-W alloys. Mater. Sci. Eng. A-Struct. Mater. Propert. Microstruct. Process. 418 (1–2), 303–311. https://doi.org/10.1016/j.msea.2005.11.046.
Sassi, W., Dhouibi, L., Berçot, P., Rezrazi, M., Triki, E., 2012. Comparative study of protective nickel-tungsten deposit behavior obtained by continuous and pulsed currents from citrate-ammonia media. Surf. Coat. Technol. 206 (19–20), 4235–4241. https://doi.org/10.1016/j.surfcoat.2012.04.030.
Giga, A., Kimoto, Y., Takigawa, Y., Higashi, K., 2006. Demonstration of an inverse Hall-Petch relationship in electrodeposited nanocrystalline Ni-W alloys through tensile testing. Scr. Mater. 55 (2), 143–146. https://doi.org/10.1016/j.scriptamat.2006.03.047.
Huang, P.C., Chou, C.C., Hsu, L.S., 2021. Preparation and tribological research of the electrodeposited Ni-W alloy coatings for piston ring application. Surf. Coat. Technol. 411. https://doi.org/10.1016/j.surfcoat.2021.126980.
Munagala, V.N.V., Wasekar, N.P., Bathini, L., Ramakrishna, L., Sundararajan, G., 2023. Deciphering the role of W content, triple junctions, and heat treatment on the corrosion performance of Ni-W alloy coatings used for automotive applications. Mater. Chem. Phys. 308. https://doi.org/10.1016/j.matchemphys.2023.128305.
Yu, Z.F., Liu, B., Li, Z.X., Liu, T.Z., Su, G., 2022. Biochar by Spirulina platensis promotes the antifouling effect of Cu2O in styrene-acrylic resin coating. Prog. Org. Coat. 168. https://doi.org/10.1016/j.porgcoat.2022.106891.
Yu, Z., Li, L., Li, Z., Su, G., Liu, T., 2024. Cu2O/Biochar-Styrene acrylic double layer composite coatings modified by NaCl: special surface and antifouling performance. Chem. Eng. Sci. 295, 120134. https://doi.org/10.1016/j.ces.2024.120134.
Chen, Q.Y., Liang, S.H., Zhang, H., Liu, D.X., Zhuo, L.C., 2021. Fabrication and characterization of W -Ni nanocomposites via a facile chemical co-precipitation route. Adv. Powder Technol. 32 (3), 908–915. https://doi.org/10.1016/j.apt.2021.01.035.
Ong, C.Y.A., Blackwood, D.J., Li, Y., 2019. The effects of W content on solid-solution strengthening and the critical Hall-Petch grain size in Ni-W alloy. Surf. Coat. Technol. 357, 23–27. https://doi.org/10.1016/j.surfcoat.2018.09.086.
Bigos, A., Wolowicz, M., Janusz-Skuza, M., Starowicz, Z., Szczerba, M.J., Bogucki, R., Beltowska-Lehman, E., 2021. Citrate-based baths for electrodeposition of nanocrystalline nickel coatings with enhanced hardness. J. Alloy. Compd. 850. https://doi.org/10.1016/j.jallcom.2020.156857.
Wasekar, N.P., Haridoss, P., Seshadri, S.K., Sundararajan, G., 2016. Influence of mode of electrodeposition, current density and saccharin on the microstructure and hardness of electrodeposited nanocrystalline nickel coatings. Surf. Coat. Technol. 291, 130–140. https://doi.org/10.1016/j.surfcoat.2016.02.024.
Lin, Y., Pan, J., Zhou, H.F., Gao, H.J., Li, Y., 2018. Mechanical properties and optimal grain size distribution profile of gradient grained nickel. Acta Mater. 153, 279–289. https://doi.org/10.1016/j.actamat.2018.04.065.
Liu, Z., Zhang, Q., Zhang, X., Yu, Z., Zhang, X., Mao, Q., Nie, J., Zhao, Y., 2024. Electrodeposition of nanocrystalline Ni and NiCr alloy coatings: Effects of Cr content on microhardness and wear resistance improvement. J. Mater. Res. Technol. 30, 3584–3593. https://doi.org/10.1016/j.jmrt.2024.04.100.
Borgia, C., Scharowsky, T., Furrer, A., Solenthaler, C., Spolenak, R., 2011. A combinatorial study on the influence of elemental composition and heat treatment on the phase composition, microstructure and mechanical properties of Ni-W alloy thin films. Acta Mater. 59 (1), 386–399. https://doi.org/10.1016/j.actamat.2010.09.045.
Yu, Z., Shi, S., Zhang, X., You, Z., Zhao, Y., 2025. Inverse Hall-Petch and nanocrystal-amorphous transition of broad-spectrum W content NiW alloys. Mater. Sci. Eng. A 943, 148774. https://doi.org/10.1016/j.msea.2025.148774.
Detor, A.J., Schuh, C.A., 2007. Microstructural evolution during the heat treatment of nanocrystalline alloys. J. Mater. Res. 22 (11), 3233–3248. https://doi.org/10.1557/Jmr.2007.0403.
Hosseini, S.N., Enayati, M.H., Karimzadeh, F., 2014. Nanoscale grain growth behaviour of CoAl intermetallic synthesized by mechanical alloying. Bull. Mater. Sci. 37 (3), 383–387. https://doi.org/10.1007/s12034-014-0672-3.
de Lima-Neto, P., Correia, A.N., Santana, R.A.C., Colares, R.P., Barros, E.B., Casciano, P. N.S., Vaz, G.L., 2010. Morphological, structural, microhardness and electrochemical characterisations of electrodeposited Cr and Ni-W coatings. Electrochim. Acta 55 (6), 2078–2086. https://doi.org/10.1016/j.electacta.2009.11.037.
Auerswald, J., Fecht, H.J., 2010. Nanocrystalline Ni-W for Wear-Resistant Coatings and Electroforming. J. Electrochem. Soc. 157 (4), D199–D205. https://doi.org/10.1149/1.3291984.
Khan, K.K., Mehmood, M., ul Hassan, M., Ahmad, J., Iqbal, Z., Muddasser, T., 2011. Gas nitriding of Electrodeposited Ni-W Alloys. Metal Sci. Heat Treatment 53 (1–2), 87–90. https://doi.org/10.1007/s11041-011-9346-6.
Hache, M.J.R., Zou, Y., Erb, U., 2024. Thermal stability of electrodeposited nanostructured high-entropy alloys. Surf. Coat. Technol. 482. https://doi.org/10.1016/j.surfcoat.2024.130719.
Cheng, X.Y., He, Y., Fan, Y., Yan, L.P., Zhou, H.L., Zhong, J.M., Li, Z.Y., Song, J.X., 2024. Strengthening the mechanical properties and corrosion resistance of Ni-W coatings by PDA-functionalized h-BN nanosheets. Diam. Relat. Mater. 141. https://doi.org/10.1016/j.diamond.2023.110567.
Nayak, B., Anwar, S., Anwar, S., 2024. Mechanical and Corrosion resistance behavior of Ultrasonication-assisted Electrodeposited Ni-SiC Nanocomposite coatings. Physica B-Condensed Matter 675. https://doi.org/10.1016/j.physb.2023.415585.
Boonyongmaneerat, Y., Saengkiettiyut, K., Saenapitak, S., Sangsuk, S., 2010. Pulse co-electrodeposition and characterization of NiW-WC composite coatings. J. Alloy. Compd. 506 (1), 151–154. https://doi.org/10.1016/j.jallcom.2010.06.162.
Li, H.J., He, Y., Luo, P.Y., Fan, Y., He, T., Zhang, Y.H., Xiang, Y.X., He, Y.H., Song, R.X., 2021. Fabrication of the ZrC reinforced Ni-W composite coating and exploration of its mechanical properties and corrosion resistance. Surf. Coat. Technol. 421. https://doi.org/10.1016/j.surfcoat.2021.127413.
Li, H.J., He, Y., Luo, P.Y., Fan, Y., Gou, L., Li, Z.J., Zhao, Y., Liu, B., He, T., Zhang, H.L., 2021. Preparation of laminar α-ZrP nanosheets enhanced Ni-W nanocomposite coating and investigation of its mechanical and anti-corrosion properties. Surf. Coat. Technol. 423. https://doi.org/10.1016/j.surfcoat.2021.127590.
Torrents, A., Yang, H., Mohamed, F.A., 2010. Effect of annealing on hardness and the modulus of elasticity in bulk nanocrystalline nickel. Metall. Mater. Trans. A-Phys. Metall. Mater. Sci. 41a (3), 621–630. https://doi.org/10.1007/s11661-009-0147-0.
Kong, J.A.T., Hache, M.J.R., Tam, J., McCrea, J.L., Howe, J., Erb, U., 2022. On the extrinsic Hall-Petch to inverse Hall-Petch transition in nanocrystalline Ni-Co electrodeposits. Scr. Mater. 218. https://doi.org/10.1016/j.scriptamat.2022.114799.
Sunwang, N., Wangyao, P., Boonyongmaneerat, Y., 2011. The effects of heat treatments on hardness and wear resistance in Ni-W alloy coatings. Surf. Coat. Technol. 206 (6), 1096–1101. https://doi.org/10.1016/j.surfcoat.2011.07.082.
Schlossmacher, P., Yamasaki, T., 2000. Structural analysis of electroplated amorphous-nanocrystalline Ni-W. Mikrochimica Acta 132 (2-4), 309–313. https://doi.org/10.1007/s006040050074.
Huang, P.-C., Chou, C.-C., Hsu, L.-S., 2021. Preparation and tribological research of the electrodeposited NiW alloy coatings for piston ring application. Surf. Coat. Technol. 411, 126980. https://doi.org/10.1016/j.surfcoat.2021.126980.

Marvel, C.J., Yin, D., Cantwell, P.R., Harmer, M.P., 2016. The influence of oxygen contamination on the thermal stability and hardness of nanocrystalline Ni-W alloys. Mater. Sci. Eng. A-Struct. Mater. Properties Microstruct. Process. 664, 49–57. https://doi.org/10.1016/j.msea.2016.03.129.

Li, S., Xianzhen, Z., Qihua, J., Zhongming, Z., Huabo, Z., 2024. Study on the corrosion resistance of electrodeposited NiW/TiO2 composite coating and its application in methylene blue degradation in simulated wastewater. Int. J. Electrochem. Sci. 19 (12), 100875. https://doi.org/10.1016/j.ijoes.2024.100875.

Li, H., He, Y., Luo, P., Xue, S., Li, Z., Cheng, X., Zhong, J., Yan, L., Fan, Y., 2022. Synthesis of ZrB2 strengthened NiW composite coating and study of its mechanical characters and anti-corrosion performance. Surf. Coat. Technol. 441, 128553. https://doi.org/10.1016/j.surfcoat.2022.128553.

Li, H., He, Y., Luo, P., Fan, Y., He, T., Zhang, Y., Xiang, Y., He, Y., Song, R., 2021. Fabrication of the ZrC reinforced NiW composite coating and exploration of its mechanical properties and corrosion resistance. Surf. Coat. Technol. 421, 127413. https://doi.org/10.1016/j.surfcoat.2021.127413.

Kumar, N., Kishore, K., Yadav, S., Sharma, P., 2024. Characterisation of Ni-Al2O3 composite coatings at different Al2O3 concentrations. Mater. Today: Proc. https://doi.org/10.1016/j.matpr.2024.06.001.

Beltowska-Lehman, E., Bigos, A., Szczerba, M.J., Janusz-Skuza, M., Maj, L., Debski, A., Wiazania, G., Kot, M., 2020. Heat treatment of ultrasonic electrodeposited Ni-W/ZrO2 nanocomposites. Surf. Coat. Technol. 393, 125779. https://doi.org/10.1016/j.surfcoat.2020.125779.